# Inclusion of Spin–Orbit and Low-Symmetry Effects in a Vibronic Coupling (PKS) Model for Mixed-Valence Dimers: Application to the Creutz–Taube Ion

**K. Neuenschwander,[†,‡] S. B. Piepho,*[§] and P. N. Schatz*[‡]**

*Contribution from the Department of Chemistry, University of Virginia, McCormick Road, Charlottesville, Virginia 22901, and Department of Chemistry, Sweet Briar College, Sweet Briar, Virginia 24595. Received May 6, 1985*

**Abstract:** The simple PKS model for mixed-valence dimers is generalized to take explicit account of both low-symmetry and spin–orbit effects. Specific application is made to a $D_{2h}$ dimer whose coupled centers, with electronic configuration $t_{2g}^5/t_{2g}^6$, have $C_{2v}$ site symmetry. The two surfaces of the simple model each split into three, the single electronic coupling parameter ($\epsilon$) is replaced by three $\epsilon$'s each of which parametrizes an interaction of different symmetry, spin–orbit coupling is introduced through the parameter $\zeta$, and the crystal field at each center is described by a tetragonal and a rhombic distortion parameter. A single vibronic coupling parameter ($\lambda$) is retained and vibronic coupling in a single effective mode is explicitly included so that "exact" solution of the dynamic problem is possible for both localized and delocalized systems. The methods for calculating $g$ values and intervalence band contours are discussed in detail. Explicit application is made to the Creutz–Taube ion; sets of parameters are sought which simultaneously simulate the experimental $g$ values and intervalence band contour. It is easy to fit the $g$ values, and a fairly unique set of parameters is found which also accounts moderately well for the intervalence band contour. However, the required $\epsilon$ values seem clearly unreasonable, and this suggests that the model is inadequate for systems with strong electronic coupling to the bridging ligand.

Since the original publication of our vibronic coupling model for dimeric mixed-valence systems (the PKS model[1]), a number of additional physical measurements have been made on the Creutz–Taube (C–T) ion, $[(NH_3)_5Ru(pyrazine)Ru(NH_3)_5]^{5+}$.[2,3]

These results have stimulated us to extend the PKS model to consider characteristics of the bridging and other liganding groups with particular emphasis on the consequent reduction of the symmetry of the metal ion centers. We make specific applications to the C–T ion.

In our original treatment, the symmetry of each metal center was taken as octahedral, and the nature of the bridging group was not considered at all. Thus the model was too simple to predict, for example, the ESR spectrum of a mixed-valence complex. The aim of our present study is to develop a model which simultaneously accounts for the three experimental $g$ values, the intervalence band shape, and the MCD spectrum. While we are only partially successful in achieving these goals, we believe that the extensions of the original PKS model described in this paper mark a significant advance.

Our present treatment takes into account the detailed symmetry of the C–T ion, and group theory is used extensively to characterize the system. The single electronic coupling parameter ($\epsilon$) used in the PKS model is replaced by three electronic coupling parameters ($\epsilon_1$, $\epsilon_2$, $\epsilon_3$) each of which parametrizes an interaction of a different symmetry. In addition, two parameters, $\Delta_{Tet}$ and $\Delta_{Rh}$, are added which measure the tetragonal and rhombic distortions, respectively, at the individual Ru centers. Consideration is taken of how the symmetry-adapted pyrazine molecular orbitals can interact with the symmetry-adapted Ru orbitals to influence the electronic coupling between the Ru centers in the dimeric complex. A single asymmetric coupling vibration and a single vibronic coupling parameter ($\lambda$) are assumed, as in the original PKS model. The roles of both the pyrazine MO's and the Ru $e_g$ orbitals are discussed with respect to the MCD.

Our new model thus adds four additional parameters and in so doing allows for a far more realistic description of the mixed-valence complex. While our discussion below is directed specifically to the C–T ion, our treatment is general and is applicable to other mixed-valence dimers. In our specific parametrizations of the C–T ion later in this paper, we start near the delocalized limit. The preponderance of evidence certainly supports

such an approach although Fürholz et al. argue that this issue has not yet been conclusively resolved.[2]

## Calculations

The symmetry of the entire C–T ion is approximately (or in some hosts exactly) $D_{2h}$ while the two individual Ru centers have $C_{2v}$ site symmetry (see Figure 1).[2] Since each Ru is surrounded by five ammonia nitrogens and one pyrazine nitrogen, the Ru centers may be viewed as distorted octahedral centers.

**Basis Chain for the Ru Centers.** Calculations for the ion are most easily performed with symmetry-adapted basis functions. Such a basis may be described by using the chain-of-groups approach of Butler[4] which is also discussed in some detail in Chapter 15 et seq. of Piepho and Schatz[5]—hereafter referred to as PS. In our present case, each Ru atom (full rotary reflection group $O_3$) is first distorted by its six adjacent nitrogens to octahedral ($O_h$) symmetry; taking into account the fact that one of these six nitrogens comes from pyrazine while the remaining five are ammonia nitrogens further lowers the symmetry to $C_{4v}$. Finally the presence of the pyrazine ring reduces the symmetry still further to $C_{2v}$. It follows from the above discussion that the group chain appropriate to the $C_{2v}$ basis functions of the Ru centers is

$$O_3 \supset O_h \supset D_{4h} \supset C_{4v} \supset C_{2v} \supset C_2 \qquad (1)$$

*Working in this basis enormously simplifies calculations.* Basis functions of the lower groups of the chain (e.g., $C_{2v}$) are also basis functions of higher groups of the chain (e.g., $O_h$). However, the particular $O_h$ basis specified by the chain in (1) is not one of the more common $O_h$ bases (e.g., it is not one of the PS bases[5]). Note in particular that on each center, the four ammonia groups adjacent to the ring are at angles of $\sim 45°$ above and below the plane of the ring[2] (see Figure 1); this leads to a different $C_{4v} \rightarrow C_{2v}$ branching than would be obtained if the pyrazine ring and two of these adjacent ammonia nitrogens lay in the same plane.

**Single-Center Basis Functions for Ru(III).** In octahedral systems (neglecting spin–orbit coupling), Ru(II) has a $t_{2g}^6$

---

† Present Address: Muhlegasse 216, 3283 Kallnach, Switzerland.
‡ University of Virginia.
§ Sweet Briar College.

(1) Piepho, S. B.; Krausz, E. R.; Schatz, P. N. *J. Am. Chem. Soc.* **1978**, *100*, 2996–3005.
(2) Fürholz, U.; Bürgi, H.-B.; Wagner, F. E.; Stebler, A.; Ammeter, J. H.; Krausz, E.; Clark, R. J. H.; Stead, M. J.; Ludi, A. *J. Am. Chem. Soc.* **1984**, *106*, 121–123 and references therein.
(3) Krausz, E.; Ludi, A. *Inorg. Chem.* **1985**, *24*, 939–943.
(4) Butler, P. H. "Point Group Symmetry Application"; Plenum Press: New York, 1981.
(5) Piepho, S. B.; Schatz, P. N. "Group Theory in Spectroscopy"; Wiley-Interscience: New York, 1983.
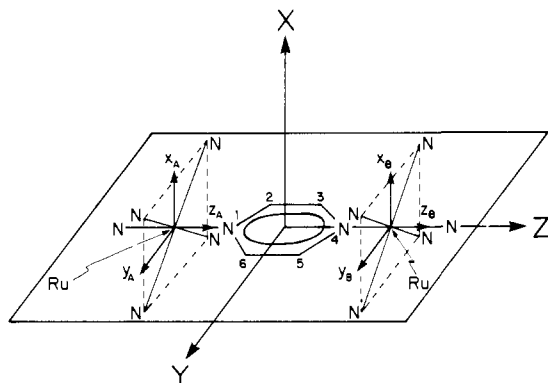(6) Wong, K. Y.; Schatz, P. N. *Prog. Inorg. Chem.* **1981**, *23*, 369–449.

**Figure 1.** Coordinate systems and structure of the Creutz–Taube (C–T) ion. The pyrazine ring is in the *YZ* plane. *X*, $x_a$, and $x_b$ are parallel as are *Y*, $y_a$, and $y_b$ and *Z*, $z_a$, and $z_b$. The *XZ* and *YZ* planes are symmetry planes of the ion. The ammonia hydrogen atoms have been omitted for clarity.

closed-shell configuration while Ru(III) has a single-hole $t_{2g}^5$ configuration; thus the ground states are respectively $^1A_{1g}$ and $^2T_{2g}$. In the chain-of-groups approach, basis states are labeled by using the branching rules for irreducible representations (irreps) of the group chain to designate the lower-group irrep to which each higher-group irrep branches when the symmetry is lowered (see PS, section 15.2 in ref 5). We have for the d oribitals of each Ru center,

$$|t_{2g}(O_h)b_3(C_{2v})\rangle \sim -iyz$$

$$|t_{2g}b_2\rangle \sim xz$$

$$|t_{2g}a_1\rangle \sim x^2 - y^2$$

$$|e_g a_1\rangle \sim -z^2$$

$$|e_g b_1\rangle \sim ixy \qquad (2)$$

On the left, irrep partners are labeled in Mulliken-type notation with their $C_{2v}$ symmetry as partner labels, and the transformation properties of the orbital in Cartesian coordinates is indicated on the right. Since Butler chooses a different $C_{2v}$ reflection plane than that dictated by the C–T ion symmetry, we may not use his $C_{4v} \rightarrow C_{2v}$ branching. Instead our $C_{4v} \rightarrow C_{2v}$ branching (and 3*jm* factors) is isomorphic with the $D_{2d} \rightarrow C_{2v}$ branching of Butler.[4]

Likewise, the single-center Ru(III) $t_{2g}^5$ basis states are

$$|\mathcal{S}hM\theta\rangle = |\tfrac{1}{2}hM\theta\rangle \text{ for } M = \pm\tfrac{1}{2} \qquad (3)$$

where $\mathcal{S}$ and $M$ designate the spin classification in $O_3$ and $h$ and $\theta$ denote respectively the spatial point group irrep and partner labels. The $|h\theta\rangle$ are given by $|T_{2g}b_3\rangle$, $|T_{2g}b_2\rangle$, and $|T_{2g}a_1\rangle$.

**Single-Center Crystal-Field Effects for Ru(III).** The tetragonal and rhombic crystal-field matrices are calculated in our $t_{2g}^5$ basis. A distortion Hamiltonian which split degeneracies of a higher group (here $O_h$) transforms as $A_{1g}$ or $A_1$ in the lower group (here $C_{4v}$ or $C_{2v}$) but not in the higher group. Thus in this case the tetragonal crystal-field operator transforms as $|E_g a_1\rangle$ and the rhombic crystal-field operator as $|T_{2g}a_1\rangle$. The matrices, which are diagonal in our basis, are easily calculated by using the equations PS (10.2.2) and PS (19.4.6) in ref 5.

Results of the perturbations are shown schematically in Figures 2 and 3 which also serve to define our parameters $\Delta_{Tet}$ and $\Delta_{Rh}$. In terms of single-electron reduced-matrix elements they are

$$\Delta_{Tet} \equiv \tfrac{1}{2}[E(T_{2g}b_2) + E(T_{2g}b_3)] - E(T_{2g}a_1)$$
$$= (3^{1/2}/2)\langle t_{2g}||V^{E_g}||t_{2g}\rangle$$

$$\Delta_{Rh} \equiv E(T_{2g}b_3) - E(T_{2g}b_2)$$
$$= (2/6^{1/2})\langle t_{2g}||V^{T_{2g}}||t_{2g}\rangle \qquad (4)$$

**Single-Center Spin–Orbit Coupling for Ru(III).** The spin–orbit matrix is calculated in the spin–orbit-coupled basis, $|(\mathcal{S}S,h)t\tau\rangle = |^1\!/_2 E_g',T_{2g})t\tau\rangle$, for $t = U_g'$ and $E_g''$. $S$ and $h$ designate group
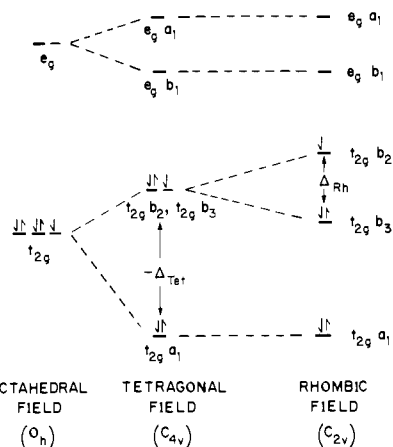


**Figure 2.** The effect of the tetragonal ($\Delta_{Tet}$) and rhombic ($\Delta_{Rh}$) crystal-field perturbations on the Ru d orbitals which are labeled as in eq 2.
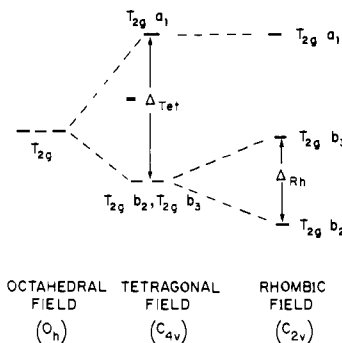


**Figure 3.** The effect of the tetragonal and rhombic crystal-field perturbations on the states of the $t_{2g}^5$ configuration of Ru(III). All states are spin doublets.

**Table I.** Single-Center Ru(III) $t_{2g}^5$ Electronic Matrix for Spin–Orbit Coupling and Crystal-Field Perturbations (Either *All* Upper or *All* Lower Signs Apply)

| $t_{2g}^5$ | $^2T_{2g} \mp \tfrac{1}{2}a_1$ | $^2T_{2g} \pm \tfrac{1}{2}b_2$ | $^2T_{2g} \pm \tfrac{1}{2}b_3$ |
|---|---|---|---|
| $^2T_{2g} \mp \tfrac{1}{2}a_1$ | $-^2\!/_3\Delta_{Tet}$ | $\pm\zeta/2$ | $-\zeta/2$ |
| $^2T_{2g} \pm \tfrac{1}{2}b_2$ | $\pm\zeta/2$ | $(^1\!/_3\Delta_{Tet} - ^1\!/_2\Delta_{Rh})$ | $\pm\zeta/2$ |
| $^2T_{2g} \pm \tfrac{1}{2}b_3$ | $-\zeta/2$ | $\pm\zeta/2$ | $(^1\!/_3\Delta_{Tet} + ^1\!/_2\Delta_{Rh})$ |

$O_h$ spin and space irreps which are coupled to form $O_h$ spin–orbit functions of irrep *t* and component *τ*. Equations PS (18.4.6) and PS (19.5.5) in ref 5 are used to calculate the spin–orbit coupling matrix elements which are diagonal in this basis. We find

$$\langle t_{2g}^5(^1\!/_2E_g',T_{2g})U_g'\tau|\mathcal{H}_{so}|t_{2g}^5(^1\!/_2E_g',T_{2g})U_g'\tau'\rangle = \delta_{\tau\tau'}(^1\!/_2\zeta)$$

$$\langle t_{2g}^5(^1\!/_2E_g',T_{2g})E_g''\tau|\mathcal{H}_{so}|t_{2g}^5(^1\!/_2E_g',T_{2g})E_g''\tau'\rangle = \delta_{\tau\tau'}(-\zeta) \qquad (5)$$

The spin–orbit matrix calculated as described above is next transformed back to the uncoupled $|\mathcal{S}hM\theta\rangle$ basis used for the crystal-field calculations. The combined single-center matrix for spin–orbit coupling and crystal-field effects is given in Table I.

**Single-Center Calculations for Ru(II).** Ru(II) has a closed-shell configuration and thus a nondegenerate, totally symmetric, ground state which is unaffected by both crystal-field and spin–orbit perturbations.

**Dimer Basis Functions.** The basis for the C–T ion ground configuration (we refer to the entire ion as the dimer, A–B) may be constructed by combining single-center Ru(III) and Ru(II) functions from centers A and B. Neglecting spin for the moment, six symmetry-adapted $D_{2h}$ states may be formed by taking linear combinations of the three states with Ru(III) on A and Ru(II) on B and the three with Ru(III) on B and Ru(II) on A. At this point we neglect contributions from pyrazine which, like Ru(II), has a closed-shell ground configuration. The symmetry labels needed to define the states arise solely from the Ru(III) centers, since the Ru(II) centers and pyrazine give only totally-symmetric

**Table II.** Definition of Electronic Coupling Parameters

| dimer state | electronic coupling energy |
|---|---|
| $\psi(A_g)$ | $-\epsilon(a_1) \equiv -\epsilon_1$ |
| $\psi(B_{2g})$ | $-\epsilon(b_2) \equiv -\epsilon_2$ |
| $\psi(B_{3g})$ | $-\epsilon(b_3) \equiv -\epsilon_3$ |
| $\psi(B_{1u})$ | $\epsilon(a_1) \equiv \epsilon_1$ |
| $\psi(B_{3u})$ | $\epsilon(b_2) \equiv \epsilon_2$ |
| $\psi(B_{2u})$ | $\epsilon(b_3) \equiv \epsilon_3$ |

contributions. It follows from our $t_{2g}^5$ basis and the $D_{2h} \rightarrow C_{2v}$ branching rules of Butler[4] that the six orbital dimer-basis states are

$$\psi(A_g) = 2^{-1/2}(|T_{2g}a_1\rangle_a + |T_{2g}a_1\rangle_b)$$

$$\psi(B_{2g}) = 2^{-1/2}(|T_{2g}b_2\rangle_a + |T_{2g}b_2\rangle_b)$$

$$\psi(B_{3g}) = 2^{-1/2}(|T_{2g}b_3\rangle_a + |T_{2g}b_3\rangle_b)$$

$$\psi(B_{1u}) = 2^{-1/2}(|T_{2g}a_1\rangle_a - |T_{2g}a_1\rangle_b)$$

$$\psi(B_{3u}) = 2^{-1/2}(|T_{2g}b_2\rangle_a - |T_{2g}b_2\rangle_b)$$

$$\psi(B_{2u}) = 2^{-1/2}(|T_{2g}b_3\rangle_a - |T_{2g}b_3\rangle_b) \qquad (6)$$

The "a" states have Ru(III) on A and Ru(II) on B and vice versa for the "b" states. Thus, for example, in the equation above

$$|T_{2g}a_1\rangle_a \equiv \psi_A(T_{2g}a_1)\psi_B(A_1a_1)$$

$$|T_{2g}a_1\rangle_b \equiv \psi_A(A_1a_1)\psi_B(T_{2g}a_1) \qquad (7)$$

and so on. Since $M = \pm^1/_2$, there are 12 states in all once spin is included. Thus, for example, including spin we have for $M = \pm^1/_2$

$$\psi(^2A_g \pm ^1/_2) = 2^{-1/2}(|^2T_{2g} \pm ^1/_2 a_1\rangle_a + |^2T_{2g} \pm ^1/_2 a_1\rangle_b) \quad (8)$$

**Electronic Coupling Perturbation for the Dimer.** The dimer-basis states of eq 6 are diagonal in the electronic coupling perturbation. Neglecting constant terms along the diagonal, the perturbation may be represented with three electronic coupling parameters—one for each $\pm C_{2v}$ combination. Thus we label these parameters by the symmetry of the $C_{2v}$ states which contribute to the dimer states involved in the electronic coupling (see Table II). Positive electronic coupling parameters define both the even-parity dimer states lower in energy and the odd-parity one-electron dimer orbitals lower in energy.

**Total Electornic Matrix for the Dimer.** The complete electronic matrix for the C–T ion including the effects of the single-center crystal-field, spin–orbit perturbations and the two-center electronic coupling perturbations is given in Table III. The magnitudes chosen for the electronic coupling parameters depend on the nature of the pyrazine bridging group.

It is important to realize that diagonalization of the electronic matrix for the dimer g states (Table III) yields three *doubly degenerate* eigenvalues, as is also the case for the dimer u states. This may readily be seen (for example, in the case of the g states) by listing the functions in the order $^2A_g + ^1/_2$, $^2B_{2g} - ^1/_2$, $^2B_{3g} - ^1/_2$, $^2A_g - ^1/_2$, $^2B_{2g} + ^1/_2$, $^2B_{3g} + ^1/_2$. Two 3 × 3 blocks result which, though not identical, can be seen by inspection to have identical eigenvalues. These double degeneracies are a reflection of the Kramers degeneracy of the system and significantly simplify subsequent calculations.

**The Role of the Pyrazine Bridge.** The electronic structure of the $\pi$ MOs of pyrazine may be estimated by using the Hückel approximation. These MOs and also the nonbonding pyrazine MOs formed from the $p_z(\sigma)$ orbitals of the pyrazine nitrogens can interact with the Ru-dimer MOs of like $D_{2h}$ symmetry. Qualitative estimates of the extent of these interactions are given in Table IV along with the form of the $\pi$ MOs. The most important interactions are clearly those which involve the $t_{2g}b_2$ atomic orbitals on the Ru centers since they are oriented for good overlap with the pyrazine $\pi$ MO's (see Figure 1). Since the electronic coupling between the dimer states of eq 6 should be greatly enhanced by the mixing of pyrazine MOs with Ru AOs, it follows that $\epsilon(b_2)$

**Table III.**[a] Dimer Matrix Elements of $\mathcal{H}_{el}$ (without Vibronic Coupling[b])

| dimer g states | $^2A_g \mp ^1/_2$ | $^2B_{2g} \pm ^1/_2$ | $^2B_{3g} \pm ^1/_2$ |
|---|---|---|---|
| $^2A_g \mp ^1/_2$ | $[-^2/_3\Delta_{Tet} - \epsilon_1]$ | $\pm\zeta/2$ | $-\zeta/2$ |
| $^2B_{2g} \pm ^1/_2$ | $\pm\zeta/2$ | $[^1/_3\Delta_{Tet} - ^1/_2\Delta_{Rh} - \epsilon_2]$ | $\pm\zeta/2$ |
| $^2B_{3g} \pm ^1/_2$ | $-\zeta/2$ | $\pm\zeta/2$ | $[^1/_3\Delta_{Tet} + ^1/_2\Delta_{Rh} - \epsilon_3]$ |

| dimer u states | $^2B_{1u} \mp ^1/_2$ | $^2B_{3u} \pm ^1/_2$ | $^2B_{2u} \pm ^1/_2$ |
|---|---|---|---|
| $^2B_{1u} \mp ^1/_2$ | $[-^2/_3\Delta_{Tet} + \epsilon_1]$ | $\pm\zeta/2$ | $-\zeta/2$ |
| $^2B_{3u} \pm ^1/_2$ | $\pm\zeta/2$ | $[^1/_3\Delta_{Tet} - ^1/_2\Delta_{Rh} + \epsilon_2]$ | $\pm\zeta/2$ |
| $^2B_{2u} \pm ^1/_2$ | $-\zeta/2$ | $\pm\zeta/2$ | $[^1/_3\Delta_{Tet} + ^1/_2\Delta_{Rh} + \epsilon_3]$ |

[a] Note that either *all* upper or *all* lower signs apply so that, for example, $(^2A_g + ^1/_2|\mathcal{H}_{el}|^2B_{2g} - ^1/_2) = -\zeta/2$ whereas $(^2A_g + ^1/_2|\mathcal{H}_{el}|^2B_{2g} + ^1/_2) = 0$. [b] To include vibronic coupling, add the term $^1/_2q^2$ to each diagonal element and couple the u and g blocks according to the following: $(^2A_g \pm ^1/_2|\mathcal{H}_{el}|^2B_{1u} \pm ^1/_2) = (^2B_{2g} \pm ^1/_2|\mathcal{H}_{el}|^2B_{3u} \pm ^1/_2) = (^2B_{3g} \pm ^1/_2|\mathcal{H}_{el}|^2B_{2u} \pm ^1/_2) = \lambda q$.

$\equiv \epsilon_2$ should be considerably larger than either $\epsilon(a_1) \equiv \epsilon_1$ or $\epsilon(b_3) \equiv \epsilon_3$.

**Vibronic Coupling and Solution of the Dynamic Problem.** As discussed in the PKS model,[1,6] the dimer vibrations which vibronically couple the different oxidation states are the odd-parity linear combinations of totally symmetric monomer vibrations—the so-called q-modes. If we treat the Ru centers as distorted octahedra, we find that five of the 15 normal vibrations on each center transform as the totally symmetric irrep in $C_{2v}$, and thus five q-modes are possible. Three of these are mainly stretching vibrations, and two include large contributions along the dimer (z) axis.

As we shall see below, solution of the electronic (static) problem,[7] i.e., determination of the potential surfaces, requires diagonalization of a 6 × 6 matrix. Solution of the dynamic problem in each case, i.e., determination of the nuclear motion on these coupled surfaces, thus involves six coupled vibronic equations.[7] Formally, we can solve this problem in exact analogy to the simple PKS procedure by expanding the unknown vibrational functions which couple these equations (the $\chi_{i\nu}$ of eq 9 below) in bases of harmonic oscillator functions in each q-mode. But use of $d$ quanta ($n = 0$ to $d - 1$) in a single q-mode produces a secular determinant of dimension $6d$, and this dimension grows exponentially with the number of q-modes used. Thus the dimension is $3d(d + 1)$ for two and $d(d + 1)(d + 2)$ for three q-modes, etc. In the present symmetrical (A = B) case, it is possible to factor the secular determinant into two sub-blocks by taking advantage of the inversion symmetry. However, it is still only practical for us to use a one-mode model. Since the vibronic coupling in the C–T ion is small in any event, this simplification should not seriously affect our analysis.

The vibronic coupling is introduced in exactly the same way as in the simple model.[6,7] $\psi_a$ and $\psi_b$ of the simple model are respectively analogous to $|T_{2g}\rangle_a$ and $|T_{2g}\rangle_b$ of eq 7. Following the treatment through, one finds the following. First, the term $(^1/_2)q^2$ must be added to each diagonal element in Table III. Second, the following non-zero elements vibronically couple the g and u functions: $(^2A_g \pm ^1/_2|\mathcal{H}_{el}|^2B_{1u} \pm ^1/_2) = (^2B_{2g} \pm ^1/_2|\mathcal{H}_{el}|^2B_{3u} \pm ^1/_2) = (^2B_{3g} \pm ^1/_2|\mathcal{H}_{el}|^2B_{2u} \pm ^1/_2) = \lambda q$. Thus each 3 × 3 g block is coupled to a corresponding 3 × 3 u block to form each of two 6 × 6 blocks (just as $\psi_+$ and $\psi_-$ are coupled in the simple model[7]). Only one of these two blocks need be considered because of the Kramers degeneracy.

Thus finally solutions to the vibronic Schrdinger equation take the form

$$\Phi_\nu = \sum_{i=1}^{6} |^2\Gamma_i\rangle|\chi_{i\nu}\rangle \qquad (9)$$

where for one of the 6 × 6 blocks, for example, $^2\Gamma_i = ^2A_g - ^1/_2$,

(7) See section III.B, p 384 et seq., ref 6.

**Table IV.** Pyrazine $\pi$ Molecular Orbitals, Hückel Approximation[a]

| MO symmetry ($D_{2h}$) | MO energy[b] ($\beta < 0$) | atomic $2P_x$ orbital coefficient[b] | | | | | | orbital occupancy | interacting Ru-dimer MO's | |
|---|---|---|---|---|---|---|---|---|---|---|
| | | $N_1$ | $C_2$ | $C_3$ | $N_4$ | $C_5$ | $C_6$ | | Ru-dimer MO $D_{2h}$ ($O_h C_{2v}$) | overlap with pyrazine MO[c] |
| $b_{3u}^{(1)}(\pi)$ | $\alpha + 2.1861\beta$ | 0.4544 | 0.3831 | 0.3831 | 0.4544 | 0.3831 | 0.3831 | 2 | $b_{3u}(t_{2g}b_2)$ | good |
| $b_{2g}^{(1)}(\pi)$ | $\alpha + 1.3508\beta$ | -0.6059 | -0.2577 | 0.2577 | 0.6059 | 0.2577 | -0.2577 | 2 | $b_{2g}(t_{2g}b_2)$ | good |
| $b_{1g}(\pi)$ | $\alpha + 1.0000\beta$ | 0 | -0.5000 | -0.5000 | 0 | 0.5000 | 0.5000 | 2 [HOMO] | $b_{1g}(e_gb_1)$ | poor |
| $b_{3u}^{(2)}(\pi^*)$ | $\alpha - 0.6861\beta$ | -0.5418 | 0.3213 | 0.3213 | -0.5418 | 0.3213 | 0.3213 | 0 [LUMO] | $b_{3u}(t_{2g}b_2)$ | good |
| $a_u(\pi^*)$ | $\alpha - 1.0000\beta$ | 0 | -0.5000 | 0.5000 | 0 | -0.5000 | 0.5000 | 0 | $a_u(c_gb_1)$ | poor |
| $b_{2g}^{(2)}(\pi^*)$ | $\alpha - 1.8508\beta$ | -0.3645 | 0.4284 | -0.4284 | 0.3645 | -0.4284 | 0.4284 | 0 | $b_{2g}(t_{2g}b_2)$ | good |
| $a_g(\pi)$ | in-phase combination of N $2P_z$ AO's | | | Pyrazine Nonbonding MO | | | | | $a_g(e_ga_1)$ | good |
| $b_{1u}(\pi)$ | out-of-phase combination of N $2P_z$ AO's | | | | | | | | $a_g(t_{2g}a_1)$ | none |

[a] Coulson, C. A.; Streitwieser, A., Jr. Dictionary of $\pi$-Electron Calculations"; W. H. Freeman & Co.: San Francisco, 1965. [b] The coordinate system is shown in Figure 1. [c] Estimated from sketches of the MO's.

$^2B_{2g} + ^1/_2$, $^2B_{3g} + ^1/_2$, $^2B_{1u} - ^1/_2$, $^2B_{3u} + ^1/_2$, $^2B_{2u} + ^1/_2$. The $|\chi_{iv}\rangle$ are then expanded in the single (one-mode model) orthonormal set of harmonic oscillator functions $\chi_n(q)$:

$$|\chi_{iv}\rangle = \sum_n c_{vn}^i \chi_n(q) \tag{10}$$

The required electronic matrix elements are already displayed in Table III, and secular equations in the $c_{vn}^i$ are obtained in exactly the same manner as in the simple model.[7] In our calculations, we employ 20 quanta in eq 10 ($n = 0$–19) so that diagonalization of a $120 \times 120$ matrix is required. Using a larger basis does not alter our results for the calculated $g$ values or intervalence band contours (see below). We did not bother in this case to use the inversion symmetry to factor the $120 \times 120$ matrix into two $60 \times 60$ matrices in analogy to the use of interchange symmetry in the simple model.[7] However, in applications to more or less strongly localized systems where significantly larger vibrational bases may be required, such factoring would be highly advantageous and indeed essential in some instances.

**EPR Simulation.** To a first approximation the Zeeman Hamiltonian for the C–T ion in an applied magnetic field $B$ is

$$
\begin{aligned}
\mathcal{H}_B &= -B \cdot \bar{\mu} \\
&= \mu_B B \cdot (L + 2S) \\
&= \mu_B B_x(L_x + 2S_x) + \mu_B B_y(L_y + 2S_y) + \mu_B B_z(L_z + 2S_z)
\end{aligned}
\tag{11}
$$

where $\mu_B$ is the Bohr magneton. The components of $\mu$, the magnetic-dipole operator, may be expressed in terms of fictitious spin–angular momentum operators $\hat{S}_i$ as[9]

$$\mu_i = -\mu_B g_i \hat{S}_i, \quad i = x, y, z \tag{12}$$

Thus the Hamiltonian becomes

$$\mathcal{H}_B = \mu_B B_x g_x \hat{S}_x + \mu_B B_y g_y \hat{S}_y + \mu_B B_z g_z \hat{S}_z \tag{13}$$

where the fictitious spin operators $\hat{S}_i$ are defined with respect to the ground-state Kramers doublet partners $|+\rangle$ and $|-\rangle$ (which move up and down respectively in a magnetic field) so that in units of $\hbar$

$$\langle +|\hat{S}_z|+\rangle = {}^1/_2, \quad \langle -|\hat{S}_z|-\rangle = -{}^1/_2$$

$$\langle +|\hat{S}_x|-\rangle = {}^1/_2, \quad \langle -|\hat{S}_x|+\rangle = {}^1/_2$$

$$\langle +|\hat{S}_y|-\rangle = -i/2, \quad \langle -|\hat{S}_y|+\rangle = i/2 \tag{14}$$

Thus the fictitious spin operator $\hat{S}_i$, $i = x, y, z$, has the same eigenvalues for the ground eigenstates $|\pm\rangle$ of the system of interest as the spin angular momentum operator $S_i$, $i = x, y, z$, has for the pure spin kets $|\pm^1/_2\rangle$. Comparing eq 11 and 13 it follows that

$$g_x = 2\langle +|(L_x + 2S_x)|-\rangle$$

$$g_y = 2i\langle +|(L_y + 2S_y)|-\rangle$$

$$g_z = 2\langle +|(L_z + 2S_z)|+\rangle \tag{15}$$

Thus to calculate the $g$ values for the C–T ion with our model we need only obtain the matrix elements of the components of $L$ and $S$ in the dimer basis (eq 6–8) and then transform the matrices using the ground-state eigenvectors to obtain ground-state $g$ values.

The magnetic moment matrix elements in the dimer basis are identical with the related matrix elements in the single-center Ru(III) basis. The single-center Ru(III) magnetic moment matrix is obtained as follows. Since spin is classified in the full rotation group $SO_3$, spin angular momentum matrix elements follow directly from standard relations. Thus nonzero results (in units of $\hbar$) are

$$\langle ^2h \pm {}^1/_2\theta|S_z|^2h' \pm {}^1/_2\theta'\rangle = \delta_{hh'}\delta_{\theta\theta'}(\pm{}^1/_2)$$

$$\langle ^2h \pm {}^1/_2\theta|S_x|^2h' \mp {}^1/_2\theta'\rangle = \delta_{hh'}\delta_{\theta\theta'}({}^1/_2)$$

$$\langle ^2h \pm {}^1/_2\theta|S_y|^2h' \mp {}^1/_2\theta'\rangle = \delta_{hh'}\delta_{\theta\theta'}(\mp i/2) \tag{16}$$

Orbital angular momentum matrix elements are found by first expressing the orbital angular momentum operator in terms of

operators which transform as irreps of our eq 1 basis chain. This is achieved by using operator transformation coefficients (PS, section 9.8 in ref 5) which are defined following the method described in section 5.3 of Butler.[4] Matrix elements of the symmetry adapted operators are then found by reduction in group $O_h$ via PS (10.2.2) followed by the use of PS (19.4.6) and PS (19.4.24).

**Simulation of the Creutz–Taube Absorption Spectrum.** The electric-dipole transition-moment matrix and the mixed-valence absorption spectrum are calculated in the same way as in the simple PKS model.[1,6] Transforming the electric-dipole operator to the monomer centers gives

$$m_x = m_x{}^A, \; m_y = m_y{}^A, \; m_z = m_z{}^A - \frac{R}{2}\sum_i e_i$$

$$m_x = m_x{}^B, \; m_y = m_y{}^B, \; m_z = m_z{}^B + \frac{R}{2}\sum_i e_i \qquad (17)$$

where $R$ is the distance between the Ru centers and $e_i$ is the charge of the $i$th electron. As long as the dimer states are the Ru-dimer states of eq 6, only the $(\pm^1/_2)Re_i$ parts contribute to the electric-dipole transition moments because of parity selection rules. Thus in this approximation only the $m_z$ matrix elements will be nonzero. Polarization studies[3] show that the $z$ intensity is by far the largest in agreement with this prediction. However, weak $x$–$y$ polarized absorption is observed[3] and the ion gives rise to a weak MCD spectrum[3] which is forbidden in the absence of some $x$ and/or $y$ intensity. A mechanism for generation of this intensity is discussed next.

**A Possible Source of $x$–$y$ Polarized Intensity of the Mixed-Valence Band.** As the C–T ion states gain pyrazine character, electric-dipole transitions centered on the pyrazine can contribute to the absorption intensity. The one-electron pyrazine transitions of importance are those to the pyrazine LUMO (lowest unoccupied MO—see Table IV):

$$\left.\begin{array}{l} b_{1g}{}^{(\pi)}[\text{HOMO}] \xrightarrow{m_y} \\[4pt] a_g(n) \xrightarrow{m_x} \\[4pt] b_{2g}{}^{(1)}(\pi) \xrightarrow{m_z} \end{array}\right\} b_{3u}{}^{(2)}(\pi)[\text{LUMO}] \qquad (18)$$

Excitations are allowed in all polarizations, but again the $z$-polarized contribution should be the most important for the C–T mixed-valence band since it involves the pyrazine MOs which mix best with the Ru-dimer MOs—see Table IV.

Mixed-valence excitations can gain $y$ polarization to the extent that (1) the metal $t_{2g}$ MOs gain $b_{1g}(\pi)$ character and (2) the metal $b_{3u}(t_{2g}b_2)$ MOs gain LUMO character. The first process can only occur indirectly as a result of interaction (via spin–orbit coupling) of $t_{2g}$ with $e_gb_1$. the $e_gb_1$ MO can in turn interact with the pyrazine HOMO, but the form of the orbitals suggests that the interaction will be weak (Table IV). This second process, however, should be important, and the HOMO-to-LUMO dipole strength is large. Thus we would expect weak $y$ polarization due to the small effect of the first process.

To obtain $x$ polarization, (1) the $t_{2g}$ MOS must gain $a_g(n)$ character and (2) the second process above must occur. For (1) to occur to any significant extent, the $t_{2g}$ orbitals must interact with the $e_ga_1$ orbitals (via spin–orbit coupling) since the $a_g(n)$ pyrazine MO can interact with the $a_g(e_ga_1)$ metal MO (Table IV). The latter interaction is expected to be moderate. But since the dipole strength of the $x$-polarized pyrazine excitation is less than that of the $y$-polarized HOMO → LUMO excitation, we expect the $x$-polarization also to be weak.

In agreement with the above qualitative arguments, the mixed-valence band is overwhelmingly $z$ polarized, the amount of $x$ polarization being of the order of 1% with the $y$ polarization somewhat larger.[3]

**Difficulty in Calculating the Magnetic Circular Dichroism (MCD) of the Mixed-Valence Band.** As mentioned above, we would expect *no* MCD to a first approximation for the C–T ion

intervalence band since MCD requires intensity in the $x$ or $y$ polarization as well as in $z$ polarization.[5] The mechanisms for generating $x$ and/or $y$ intensity described above could account for the weak MCD observed. But explicit calculation of the MCD for those mechanisms is a formidable task which we do not attempt here. Such a calculation would require both a full MO treatment of the complex *and* the addition to the Ru basis sets of states of the higher-energy $t_{2g}{}^n e_g{}^m$ configurations.

**Results**

The goal of the present study is a model for the C–T ion which gives a unified explanation of as many experimental results as possible with detailed emphasis on the observed $g$ values and intervalence absorption profile. We find that it is easy to simulate the $g$ values. Wide ranges of parameters will accomplish this task (see below). It is also possible to reasonably simulate the intervalence band contour by appropriate choices of parameters. But the challenge and opportunity is to find a set of parameters *which accomplishes both tasks simultaneously.* We now show the extent to which we can do this and discuss the implications and uniqueness of the results.

$g$ **Values.** The $g$ values for the C–T ion are now accurately known:[2,8]

$$g_x = 1.346 \qquad g_y = 2.799 \qquad g_z = 2.487 \qquad (19)$$

The expressions needed to calculate these quantities are given in eq 15, where $\pm$ there designates the two components of the lowest energy Kramers doublet described by eq 9. Thus we must choose values of the seven parameters ($\Delta_{\text{Tet}}$, $\Delta_{\text{Rh}}$, $\epsilon_1$, $\epsilon_2$, $\epsilon_3$, $\zeta$, $\lambda$), carry out the diagonalizations previously described, substitute the resulting eigenfunctions into eq 15, and compare with experiment.

To reduce the number of parameters, we will choose $\zeta = 1000$ cm$^{-1}$ and $\lambda = 1.1$. The former choice is quite reasonable for $\zeta_{4d}(\text{Ru})$,[10] and the latter has been obtained by comparing the Ru–N distances in the Ru$^{2+}$ and Ru$^{3+}$ hexammines.[11] These choices allow us to focus on the least understood parameters—the three $\epsilon$'s and two $\Delta$'s.

We can get a good rough guide for our choice of these remaining parameters in the following way. Let us first neglect vibronic coupling entirely by setting $\lambda = 0$. The g states (upper block Table III) lie lower than the u states because we have defined our $\epsilon$'s (arbitrarily) to be positive. (Note that this is opposite the convention used in the simple PKS model.[1,6]) Inspection of Table III then shows that each Kramers doublet from the g block (and therefore the ground-state doublet) has the form

$$|\pm\rangle = a|^2A_g - \tfrac{1}{2}\rangle + b|^2B_{2g} + \tfrac{1}{2}\rangle + c|^2B_{3g} + \tfrac{1}{2}\rangle$$

$$|\mp\rangle = a|^2A_g - \tfrac{1}{2}\rangle - b|^2B_{2g} + \tfrac{1}{2}\rangle + c|^2B_3g + \tfrac{1}{2}\rangle \qquad (20)$$

Thus via eq 15, the $g$ values are now entirely determined by the coefficients $a$, $b$, and $c$ in eq 20. Let us now for convenience add the quantity $(\epsilon_1 + \epsilon_2 + \epsilon_3)/3$ to each diagonal element in the g block (Table III) noting that this cannot change the values of $a$, $b$, and $c$ in eq 20. We designate these new diagonal elements as $d_1$, $d_2$, and $d_3$ and thus write,

$$d_1 = -\tfrac{2}{3}\Delta_{\text{Tet}} - \tfrac{2}{3}\epsilon_1 + \tfrac{1}{3}\epsilon_2 + \tfrac{1}{3}\epsilon_3$$

$$d_2 = \tfrac{1}{3}\Delta_{\text{Tet}} - \tfrac{1}{2}\Delta_{\text{Rh}} + \tfrac{1}{3}\epsilon_1 - \tfrac{2}{3}\epsilon_2 + \tfrac{1}{3}\epsilon_3$$

$$d_3 = \tfrac{1}{3}\Delta_{\text{Tet}} + \tfrac{1}{2}\Delta_{\text{Rh}} + \tfrac{1}{3}\epsilon_1 + \tfrac{1}{3}\epsilon_2 - \tfrac{2}{3}\epsilon_3 \qquad (21)$$

The numerical values of $d_1$, $d_2$, and $d_3$ (in units of $\zeta$) now determine $a$, $b$, and $c$ and thus the g values (still holding $\lambda = 0$). By trial and error we find that the values $3d_1 = 1.25\zeta$, $3d_2 = -4.75\zeta$, $3d_3 = 3.5\zeta$ work quite well, giving the g values $g_x = 1.37$, $g_y = 2.81$, $g_z = 2.50$. Substituting these values for $d_1$, $d_2$, and $d_3$ into eq 21 and solving, we get the desired relations:

$$\Delta_{\text{Tet}} = -\tfrac{1}{2}[1.25\zeta + 2\epsilon_1 - \epsilon_2 - \epsilon_3]$$

$$\Delta_{\text{Rh}} = -\tfrac{2}{3}[-4.75\zeta - \Delta_{\text{Tet}} - \epsilon_1 + 2\epsilon_2 - \epsilon_3] \qquad (22)$$

(8) Stebler, A.; Ammeter, J. H.; Fürholz, U.; Ludi, A. *Inorg. Chem.* **1984**, *23*, 2764–2767.

**Table V.** Parameters Used and Calculated $g$ Values[a]

| | I | II | III[b] | IV | V | VI | VII[c] | VIII | IX | exptl[d] |
|---|---|---|---|---|---|---|---|---|---|---|
| $\Delta_{Tet}$ (cm$^{-1}$) | 0 | -1100 | 843.8 | -600 | -800 | -600 | 0 | -600 | -800 | |
| $\Delta_{Rh}$ (cm$^{-1}$) | 0 | 0 | -109.2 | 2690 | 1600 | 800 | 0 | 1800 | 2200 | |
| $\zeta$ (cm$^{-1}$) | 1000 | 1000 | 1000 | 1000 | 1000 | 1000 | 1000 | 1000 | 1000 | |
| $\lambda$ | 1.1 | 1.1 | 1.1 | 1.1 | 1.1 | 1.1 | 1.1 | 3.0 | 4.0 | |
| $\epsilon(a_1) \equiv \epsilon_1$ (cm$^{-1}$) | 875 | 2225 | 0 | 3080 | 2870 | 2000 | 3080 | 2720 | 2820 | |
| $\epsilon(b_2) \equiv \epsilon_2$ (cm$^{-1}$) | 2875 | 3125 | 2900 | 3080 | 3250 | 3000 | 3080 | 3320 | 3000 | |
| $\epsilon(b_3) \equiv \epsilon_3$ (cm$^{-1}$) | 125 | 375 | 0 | 3080 | 2120 | 1050 | 3080 | 2070 | 1270 | |
| $g_x$ | 1.34 | 1.36 | 1.33 | 1.34 | 1.36 | 1.36 | 2.0 | 1.36 | 1.35 | 1.346 |
| $g_y$ | 2.81 | 2.80 | 2.81 | 2.82 | 2.81 | 2.81 | 2.0 | 2.81 | 2.81 | 2.799 |
| $g_z$ | 2.50 | 2.51 | 2.47 | 2.50 | 2.50 | 2.50 | 2.0 | 2.49 | 2.50 | 2.487 |

[a] $h\nu = 500$ cm$^{-1}$, $T = 4.2$ K, $d = 20$ quanta; orbital reduction factor is 1.0 except 0.98 for III. [b] Dubicki et al. parameters, ref 13; note that because of the inclusion of vibronic coupling here the calculated $g$ values differ a little from those in ref 13. The latter could easily be recovered by fine tuning the parameters—see text. [c] Simple PKS model. [d] References 2 and 8.
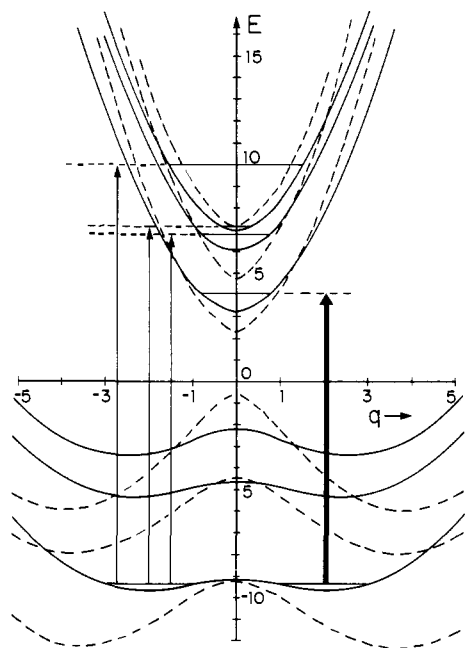


**Figure 4.** Solid curves are the potential surfaces for a slightly localized case (Table V, column VIII). The vertical arrows show the most intense vibronic transitions which occur "between" the potential surfaces. Energies are in units of $h\nu = 500$ cm$^{-1}$. The dashed curves show a more strongly localized case (Table V, column IX).

Columns I, II, V, and VI of Table V show the results of calculations using parameters which satisfy eq 22 exactly. These four columns would thus all give exactly the $g$ values quoted just above if $\lambda$ were zero. The actual values differ and thus reflect the inclusion of vibronic coupling ($\lambda = 1.1$). But the important point to note is that the changes which occur when the vibronic coupling is included are small because the vibronic coupling in the present case is small ($\lambda = 1.1$). Thus eq 22 gives a remarkably accurate description of the way in which $\zeta$, the two $\Delta$'s, and the three $\epsilon$'s must be interrelated if the experimental $g$ values of the C–T ion are to be recovered (approximately) from the model.

It is clear from eq 22 that *very great* latitude is possible in choosing parameter sets which account for the observed $g$ values. Thus it is evident that statements[12] about the state of delocalization (or localization) of the C–T ion *based solely on observed g values* are unsupportable. This is illustrated in Table V where good agreement with the experimental $g$ values is obtained for a slightly localized (column VIII) and more strongly localized case (column
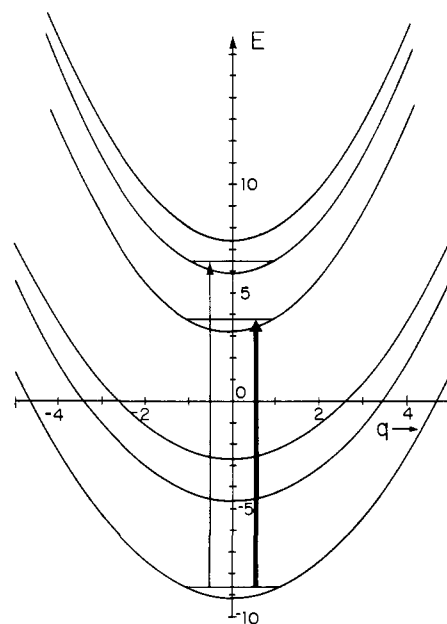
(9) Griffith, J. S. "The Theory of Transition-Metal Ions"; Cambridge University Press: London, 1964; Section 12.3.2.

(10) Collingwood, J. C.; Schatz, P. N.; McCarthy, P. *J. Mol. Phys.* **1975**, *30*, 469–491.

(11) See Section V.D., p 425 et seq., ref 6.

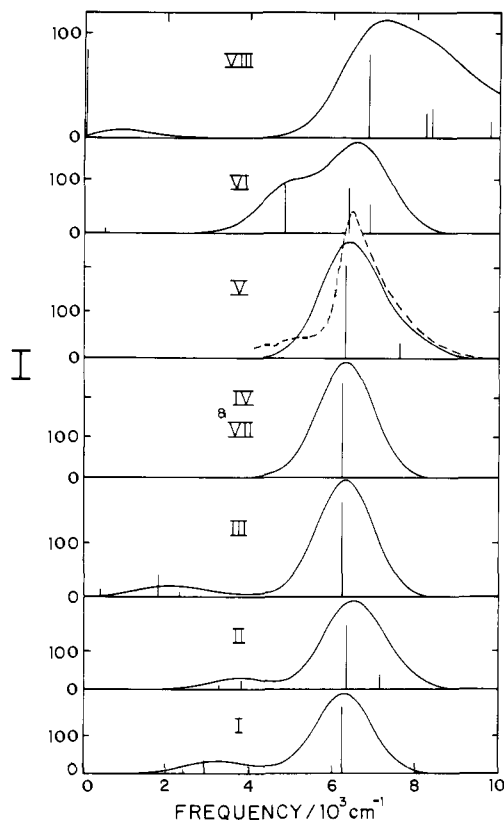(12) Hush, N. S.; Edgar, E.; Beattie, J. K. *Chem. Phys. Lett.* **1980**, *69*, 128–133.



**Figure 5.** Potential surfaces for the "best fit" case (Table V, column V). Notation as in Figure 4.

IX), as well as for a variety of delocalized cases (columns I–VI). The potential surfaces for the localized cases and for our "best fit" case (Column V, see below) are displayed in Figures 4 and 5, respectively. (These surfaces have been generated by diagonalizing, as a function of $q$, either of the Kramers degenerate 6 × 6 matrices which result when the g and u blocks of Table IV are vibronically coupled—for example, $^2A_g - ^1/_2$, $^2B_{2g} + ^1/_2$, $^2B_{3g} + ^1/_2$, with $^2B_{1u} - ^1/_2$, $^2B_{3u} + ^1/_2$, $^2B_{2u} + ^1/_2$ as described earlier in the subsection on vibronic coupling and the dynamic problem.) Clearly, the detailed interrelations among crystal-field, electronic, and vibronic coupling effects must be considered if one is to calculate the correct $g$ values *and* draw conclusions about degree of delocalization. This in turn requires a detailed analysis of the intervalence band contour since different parameter sets (Table V) predict different spectra. In fact, in our model the issue of delocalization rests crucially on the magnitude assumed for the vibronic coupling. If one is willing to assign $\lambda$ a value around 1.1 based on bond length considerations,[11] the conclusion that the C–T ion is delocalized is simply inescapable if one is also to account for a strong intervalence band around 6000 cm$^{-1}$. The precise $g$ values really have little direct bearing on this *qualitative* issue.

**Intervalence Band Contour.** We start with several general observations. First, note that if $\epsilon_1 = \epsilon_2 = \epsilon_3$, then the calculated $g$ values are independent of $\epsilon$ in which case for $\zeta = 1000$ cm$^{-1}$, $\Delta_{Tet}$ and $\Delta_{Rh}$ are fixed by the experimental $g$ values at about $-600$ and $+2700$ cm$^{-1}$, respectively (column IV, Table V). That this must be so is evident from the form of the Table III matrices since their eigenvalues must be invariant to a constant additive factor along the diagonal. The simple PKS model is the special isotropic case $\epsilon_1 = \epsilon_2 = \epsilon_3$ *and* $\Delta_{Tet} = \Delta_{Rh} = 0$ (column VII) and can only

**Figure 6.** Simulated intervalence band contours in arbitrary absorbance units vs. frequency ($\nu$) using the formula $I(\nu) = (\text{constant}) \cdot \nu \sum_i D_i f_i(\nu)$. $D_i$ is the dipole strength (transition moment squared) for the $i$th transition whose line shape is given by the normalized Gaussian, $f_i(\nu) = (1/\Delta \pi^{1/2}) \exp[-(\nu - \nu_i)^2/\Delta_i^2]$. *Relative* intensities within and between panels are correct, and the more important $D_i$ are shown by proportional vertical bars. The Roman numerals correspond to the columns in Table V. All $\Delta_i$ where chosen to be 950 cm$^{-1}$ excpet 1100 cm$^{-1}$ was used in VIII. The experimental contour in a PVA film at low temperature is shown in V by the dashed curve which is reported[3] to have a molar extinction coefficient of 9500 at the band maximum vs. a solution value of 5500.

give $g_x = g_y = g_z = 2.0$; it thus utterly fails to simulate the observed ESR results. In addition, if $\epsilon_1 = \epsilon_2 = \epsilon_3$, the intervalence absorption spectrum does *not* depend *at all* on the crystal-field parameters, $\Delta_{\text{Tet}}$ and $\Delta_{\text{Rh}}$, *or* on the spin–orbit coupling parameter $\zeta$. This follows from the form of the matrices in Table III—the u and g blocks have identical off-diagonal elements, and corresponding diagonal elements differ by $2\epsilon$. The *form* of the eigenvectors in the u and g blocks will be identical. The three *pairs* of surfaces between which intervalence transitions are then restricted will all have exactly the same separation—roughly $2|\epsilon|$ for small $\lambda$.

As soon as the $\epsilon$ values are chosen unequal, the spectrum becomes dependent on the spin–orbit *and* the crystal-field parameters, as well as on the $\epsilon$ values. We thus explore this general case with the aim of fitting *both* the observed $g$ values and intervalence band. (We note that in this case it is possible by sufficient trial and error to bring the $g$ values arbitrarily close to experiment by fine tuning the various parameters. We have in general been content to bring the $g$ values to within $\sim 0.01$–0.02 of experiment.) Table V and Figure 6 summarize typical cases; panel V of the latter which corresponds to column V of the former shows our "best fit" to the low-temperature C–T ion intervalence spectrum (also shown) which has been measured in a PVA film in the most careful experimental study to date.[3] Theoretical contours are produced by assigning a fixed ad hoc width to each transition (caption, Figure 6). Except for the column V case, the attempted fits fail qualitatively in various ways. The column I, III, IV and VII cases show no asymmetry in the main band and the column I and III cases also predict substantial absorption below 4000 cm$^{-1}$ which has not been observed. The column III case shows insufficient asymmetry on the high energy side of the main band

although the lower energy band at $\sim 3800$ cm$^{-1}$ is moving close to the region where absorption is actually observed (see dashed curve, panel V). The column VI case shows the asymmetry on the wrong side of the band and the slightly localized case (column VIII) shows far too much absorption on the high energy side. The more strongly localized case (column IX) predicts a spectrum which bears little resemblance to experiment and is not shown.

**Discussion**

We have been able to find a set of parameters (column V, Table V) which reproduce the $g$ values well and the intervalence band tolerably well, and this is gratifying. Furthermore, $\epsilon_2 (\equiv \epsilon(b_2))$, which should be dominant because of the mixing of Ru and pyrazine MO's (Table IV), is the largest of our three $\epsilon$'s. *On the other hand,* our $\epsilon_1 (\equiv \epsilon(a_1))$ value is almost 90% of $\epsilon_2$ and $\epsilon_3 (\equiv \epsilon(b_3))$ is very far from negligible, whereas qualitative arguments (Table IV) suggest that $\epsilon_1$ should be much smaller than $\epsilon_2$ with $\epsilon_3$ still smaller. Thus while the $\epsilon$ values go in the expected order, the latter two seem much too large, and this suggests a fundamental inability of our model to deal with this bridged (almost certainly), strongly delocalized system. We reiterate that it is simply not possible with the present model to simulate the mixed-valence absorption region (and the experimental $g$ values) with only $\epsilon_2$ large. This is illustrated by the column III case (Table V), which uses the parameters of Dubicki et al.[13] These workers have recently reported a theoretical study of the ESR and intervalence spectra of the C–T ion. Making the identifications (their symbols on the left) $\Delta = \Delta_{\text{Tet}}$, $\beta = \Delta_{\text{Rh}}$, $W = \epsilon_2 h\nu$, their electronic matrix is consistent with our Table III results. They assume $\epsilon_1 = \epsilon_3 = 0$; they also do not include vibronic coupling in their treatment. We note that the Dubicki et al. intervalence spectrum (Figure 6, panel III) is unsatisfactory. Significant intensity is predicted at $\sim 2000$ cm$^{-1}$ which is not experimentally observed, as noted by Dubicki et al. But in addition, their main intervalence band at 6200 cm$^{-1}$ is symmetrical because it is the result of a single electronic transition, and hence it cannot show the asymmetry on the high energy side which is so characteristic of the C–T ion band. These problems are an inevitable feature of all simulations which assume that only one of the three electronic couplings is important.

It is also disappointing that we cannot hope to simulate the observed MCD spectrum with the present model, despite the presence of 7 parameters! To calculate properly the required $x$ and/or $y$ polarization requires a full MO treatment of the complex *and* the inclusion of higher energy $t_{2g}^n e_g^m$ configurations. This is a very important and formidable task. We note the recent work in this direction by Ondrechen et al.[15]

Our best fit case (Column V, Table V) appears to be fairly unique. Appreciable variations in the parameters decrease the quality of the fit to experiment. But it is difficult to make this statement quantitative, especially in regard to the intervalence band. We suspect that the distinctive shape of the latter is not apt to be simulated by any one-mode model, and thus what constitutes the criterion for a best fit is somewhat subjective. We content ourselves with the observation that we could find no other general regime of parameters that does as well as those in column V.

It is interesting to note that our best fit case uses a rhombic distortion which is twice the magnitude of the tetragonal distortion parameter. This in fact is the relation adopted by Hush et al. in their earlier treatment.[12] That treatment, however, effectively used a single-ion model. In particular, electronic coupling ($\epsilon$) was neither explicitly included nor distinguished from crystal field effects, and no attempt was made to simultaneously fit the intervalence band contour. (Recall that if all three $\epsilon$'s are chosen equal, the $g$ values require $|\Delta_{\text{Rh}}| \sim 4.5 |\Delta_{\text{Tet}}|$—column IV, Table V.) Thus the fact that both treatments employ the same ratio of crystal field parameters seems to us fortuitous.

(13) Dubicki, L.; Ferguson, J.; Krausz, E. R. *J. Am. Chem. Soc.* **1958**, *107*, 179–182.
(14) See Table 4, ref 13.
(15) Ondrechen, M. J.; Ellis, D. E.; Ratner, M. A. *Chem. Phys. Lett.* **1984**, *109*, 50–55.

## Conclusions

We have generalized the simple PKS model to include explicitly both crystal-field and spin–orbit effects. This has been done in a systematic manner by using the Butler chain-of-groups approach. All matrix elements have been explicitly given so that direct application of the model to other symmetrical dimer systems is possible. Vibronic coupling has been explicitly included. As compared to the simple model, it is necessary to diagonalize matrices three times larger for a given vibrational basis. However, even strongly localized systems, which require large basis sets, can be easily handled with the computing power now routinely available. Of course the effects of vibronic coupling become increasingly pronounced as the system becomes increasingly localized.

We have pushed our model to the logical limit in analyzing the ESR and optical data available on the C–T ion, and the model has been found wanting. While it can simulate these data reasonably well, the electronic coupling parameters ($\epsilon_1$, $\epsilon_2$, $\epsilon_3$) required are clearly unreasonable both on qualitative grounds and on the basis of detailed calculations.[15] It is possible that adding additional q-modes could help. In the case of the simple model, the addition of a second effective ("solvent") mode did add breadth to the high-energy side of the intervalence band in a plausible way.[16] In addition, the model really requires three distinct $\lambda$ values, but this should not be a significant factor for the C–T ion because vibronic coupling is small in any event. We suspect that the problem is more fundamental, namely that the model in its present form simply does not take adequate account of the bridging ligand (the pyrazine ring) which must play a vital role in this strongly coupled system. In this regard, we note the recent very interesting work of Ondrechen and co-workers[15,17-19] which explicitly includes

the bridging ligand in a three-site model (as opposed to our two-site model). A very important feature of her work is the explicit argument that the $q_+$ mode(s) play a vital and indeed even dominating role in systems in which the electronic coupling to the bridging ligand is sufficiently strong. (Such modes are decoupled from the problem to a very good approximation in the two-site model.[16])

It seems to us that a clear opportunity is present to attempt a synthesis of our present treatment and the three-site model of Ondrechen. The latter at present neglects spin–orbit coupling and does not explicitly consider the tetragonal and rhombic distortion parameters. It therefore cannot be used to calculate g values. It would clearly be of great interest to explicitly include the pyrazine bridge in our present treatment in the manner developed by Ondrechen et al. We have high hopes that in this way it will prove possible to rationalize the g values and intervalence band contour with sensible parameters, i.e., with $\epsilon_2$ large and $\epsilon_1$ and $\epsilon_3$ small or negligible. We hope to pursue this point in future work. Such an approach may also suggest a framework for a detailed analysis of the MCD spectrum.[3]

Finally, we note that as the role of the bridging ligand diminishes, as for example in more localized systems, our present treatment becomes increasingly applicable. Obviously, examination of specific cases is required to test its usefulness.

(16) Wong, K. Y.; Schatz, P. N. "Mechanistic Aspects of Inorganic Reactions"; Rorabacher, D. B., Endicott, J. F., Eds.; American Chemical Society: Washington, D.C., 1982; Am. Chem. Soc. Symp. Ser. 198, pp 281–299.

(17) Root, L. J.; Ondrechen, M. J. *Chem. Phys. Lett.* **1982**, *93*, 421–424.
(18) Ondrechen, M. J.; Ko, J.; Root, L. J. *J. Phys. Chem.* **1984**, *88*, 5919–5923.
(19) Ko, J.; Ondrechen, M. J. *Chem. Phys. Lett.* **1984**, *112*, 507–512.

# Theoretical Studies of the System $H_3O^+(H_2O)_n$ for $n = 1-9$

**E. Kochanski***

*Contribution from E.R. n° 139 du CNRS, Université Louis Pasteur, Strasbourg, France. Received March 7, 1985*

**Abstract:** Monte Carlo calculations have been performed on the system $H_3O^+(H_2O)_n$ for $n = 1-9$, using approximate expressions to describe the interaction between $H_3O^+$ and $H_2O$ and between two water molecules (MCY potential). The cluster formation energies through the reaction $H_3O^+(H_2O)_{n-1} + H_2O \rightleftharpoons H_3O^+(H_2O)_n$ are evaluated and compared to experimental data. Interesting information about the structure and the filling of the different solvation shells of water around $H_3O^+$ is obtained. In particular, we can note a tendency for large $n$, to fill the first shell with a fourth water molecule and to fill a third shell before the second one is complete.

## I. Introduction

Since its existence was postulated in 1907,[1] the structure of $H_3O^+$ has been rather extensively discussed (see for instance ref 2–4). Many experimental data are available on crystalline hydrates of strong acids[5] or liquids[3,6] concerning $H_3O^+$ only, more recent work often being extended to larger systems $H^+(H_2O)_n$ in

solids,[4,7-10] liquids,[11-13] or gas phase.[14-24] Parallel to this work in laboratory, observations in the stratosphere and lower tropo-

*Address correspondence to this author at the Laboratoire de Chimie Théorique, Institut de Chimie, 1, rue Blaise Pascal, B.P. 296/R8, 67008 Strasbourg Cedex, France.

(1) H. Goldschmidt and O. Udby, *Z. Phys. Chem.*, **60**, 728 (1907).
(2) W. R. Rodwell and L. Radom, *J. Am. Chem. Soc.*, **103**, 2865 (1981).
(3) G. D. Mateescu and G. M. Benedikt, *J. Am. Chem. Soc.*, **101**, 3959 (1979); M. C. R. Symons, *J. Am. Chem. Soc.*, **102**, 3982 (1980).
(4) J. P. Behr, Ph. Dumas, and D. Moras, *J. Am. Chem. Soc.*, **104**, 4540 (1982).